Spin-charge filtering through a spin-orbit coupled quantum dot controlled via an Aharonov-Bohm interferometer

R. J. Heary, J. E. Han, and Lingyin Zhu
Department of Physics, State University of New York at Buffalo, Buffalo, New York 14260, USA
(Received 12 April 2007; revised manuscript received 19 November 2007; published 25 March 2008)

We show that a strongly correlated quantum dot embedded in an Aharonov-Bohm interferometer can be used to filter both charge and spin at zero voltage bias. The magnitude with which the Aharonov-Bohm arm is coupled to the system controls the many-body effects on the quantum dot. When the quantum dot is in the Kondo regime, the flow of charge through the system can be tuned by the phase of the Aharonov-Bohm arm, φ_{AB}. Furthermore, when a spin-orbit interaction is present on a Kondo quantum dot, we can control the flow of spin by the spin-orbit phase, φ_{SO}. The existence of the Kondo peak at the Fermi energy makes it possible to control the flow of both charge and spin in the zero voltage bias limit.

DOI: 10.1103/PhysRevB.77.115132 PACS number(s): 73.23.−b, 85.35.−p, 85.75.−d

I. INTRODUCTION

The ability to easily control charge and spin transport is of great importance in nanotechnology, specifically spintronics. The quantum dot Aharonov-Bohm interferometer (QD-ABI) (Fig. 1) has been found to be a candidate for manipulating electron spins.[1,2] In recent years, a number of theories[3–5] have been put forth to take advantage of the interference effects in such a geometry. Sun and Xie[1] showed that the spin polarization on the QD may be controlled via the voltage bias. In the presence of a local Coulomb interaction on the QD, Hofstetter *et al.*[3] studied the dependence of the Fano line shape on the AB phase.

In this paper, we show that the addition of a spin-orbit (SO) interaction on the strongly correlated QD allows the QD-ABI to function as a spin-charge filter. The ability of this system to act as a filter is a consequence of the interference between the continuum (AB arm) and the localized state (QD), which is known as the Fano effect.[6] Aside from the QD-ABI, the Fano effect has been observed in a single electron transistor,[7] a quantum wire with a side coupled QD,[8,9] and multiwall carbon nanotubes in a crossed geometry.[10]

The presence of the AB arm tends to localize electrons on the QD, depending on how strongly the arm is coupled to the system. Therefore, this property will give us an effective control over the strength of these correlations on the QD. We may exploit this tuning of the many-body physics to control the charge-spin transport of the QD-ABI system.

The QD interactions we will study in this paper are an on-site Coulomb interaction and the Rashba spin-orbit interaction.[11] The Coulomb interaction in the Kondo regime will allow us to filter both charge and spin at zero bias. The reason for this is due to the fact that the Kondo effect induces a sharp resonance in the QD spectral function at the Fermi energy. The further addition of the SO interaction, which is induced by the application of a gate potential, for a single orbital QD, will create a spin dependent phase factor[2] in the AB arm tunneling coefficient.

Often the spin-orbit interaction is considered a coupling with spin degrees of freedom mediated by interlevel transitions in quantum dot systems and therefore, due to the significant level spacing and the Coulomb interaction, the interlevel SO coupling strengths in QD systems are thought to be small. However, as pointed out in Ref. 2, an intralevel phase factor induced by the SO coupling may be realized in systems with high g-factors[12] such as InGaAs quantum dots. Without the interference effect, e.g., without the AB arm, such effect can be ignored. However, the presence of the AB arm not only manifests the intralevel SO interference effects, but also effectively controls the many-body effects on the QD, hence a strong influence on the charge-spin transport.

The experimental setup of the QD-ABI is consistent with that of Kobayashi *et al.*[13] The left and right leads are modeled as infinite noninteracting electron reservoirs. They are connected to each other via two arms. The top arm is the AB arm which has a complex tunneling coefficient $t_0=|t_0|e^{i\varphi_{AB}}$ that is controlled by a magnetic field. The sign of φ_{AB} is defined as positive for electrons traveling from the left reservoir to the right reservoir. We consider the magnetic field to be small enough so that we may ignore the Zeeman splitting of the QD energy level. The bottom arm contains the embedded QD with real tunneling coefficients t_L and t_R. We choose t_L, t_R to be real because the L, R states are defined to absorb the phase factor. Our calculations are carried out in the low-bias, linear response regime.

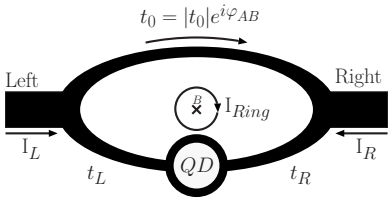

FIG. 1. Experimental setup of the quantum dot embedded AB interferometer. Two infinite electron reservoirs (Left, Right) are connected by two arms. The bottom arm contains the embedded QD with real tunneling coefficients t_L and t_R. The upper arm is a direct connection between the left and right leads with a complex tunneling coefficient $t_0=|t_0|e^{i\varphi_{AB}}$, where φ_{AB} is a phase factor controlled by the magnetic field, B. The sign of φ_{AB} is positive for electrons traveling from the left to the right, as the arrow indicates. I_L, I_R, and I_{Ring} are the Left, Right, and Ring currents, respectively.

 ©2008 The American Physical Society

II. THEORY

A. Transmission coefficient $T(\epsilon)$

In this section of the paper, we will derive the general transport functions for the QD-ABI, which are valid for a local interaction on the QD. The noninteracting Hamiltonian of the system is given by

$$\mathcal{H} = \mathcal{H}_{L,R} + \mathcal{H}_d + \mathcal{H}_t. \tag{1}$$

The Hamiltonian $\mathcal{H}$ consists of three parts: $\mathcal{H}_{L,R}$ describes the reservoirs, $\mathcal{H}_d$ the QD, and $\mathcal{H}_t$ the tunneling between the reservoirs.

$$\mathcal{H}_{L,R} = \sum_{\alpha k\sigma} \epsilon_{\alpha k} c^\dagger_{\alpha k\sigma} c_{\alpha k\sigma}, \tag{2}$$

$$\mathcal{H}_d = \sum_{\sigma} \epsilon_d d^\dagger_\sigma d_\sigma, \tag{3}$$

$$\mathcal{H}_t = -\frac{1}{\sqrt{\Omega}} \sum_{\alpha k\sigma} t_\alpha (c^\dagger_{\alpha k\sigma} d_\sigma + \text{H.c.}) - \frac{1}{\Omega} \sum_{k,k'} (t_0 c^\dagger_{Lk\sigma} c_{Rk'\sigma} + \text{H.c.}), \tag{4}$$

where $c^\dagger_{\alpha k\sigma}$ ($c_{\alpha k\sigma}$) and $d^\dagger_\sigma$ (d_σ) are the creation (annihilation) operators with momentum k and spin σ of the $\alpha=(L,R)$ reservoir and the QD, respectively. In addition, Ω is the volume of the reservoirs, which is taken to infinity.

Before presenting the Landauer formula for the current, we define the parameters. In the noninteracting limit without the AB arm, the line broadening of the QD spectral function due to the leads is $\Gamma=\Gamma_L+\Gamma_R$, where $\Gamma_\alpha=\pi N_0 t_\alpha^2$. In our calculations, we take the density of states, N_0, to be a constant.

The current from the L to R reservoir, regardless of the local interaction on the QD, is expressed by the Landauer formula,[14]

$$I_L = \frac{2e^2}{h} \int_{-\infty}^{\infty} T(\epsilon) \Delta f(\epsilon) d\epsilon. \tag{5}$$

Here, $\Delta f(\epsilon)=f_L(\epsilon)-f_R(\epsilon)$, and $T(\epsilon)$ is the transmission function. The transmission function was previously reported in Refs. 3 and 4, although without derivation. Therefore, we present the derivation, which makes use of standard Keldysh Green function techniques,[15,16] in the Appendix. Here, we summarize the results.

The transmission function may first be decoupled into two parts, the flow of current through the QD and through the AB arm,

$$T(\epsilon)\Delta f = i_{\text{QD}}(\epsilon) + i_{\text{AB}}(\epsilon),$$

$$i_{\text{QD}}(\epsilon) = -t_L(G^<_{dL}(\epsilon) - G^<_{Ld}(\epsilon)) = 2\,\text{Re}[-t_L G^<_{dL}(\epsilon)],$$

$$i_{\text{AB}}(\epsilon) = [-t_0^* G^<_{RL}(\epsilon) + t_0 G^<_{LR}(\epsilon)] = 2\,\text{Re}[-t_0^* G^<_{RL}(\epsilon)], \tag{6}$$

where we have used the relation, $G^<_{\alpha\beta}=-(G^<_{\beta\alpha})^*$. i_{QD} and i_{AB} are the contributions to the current from the QD and the AB arm, respectively. To simplify our notation, we define the following parameters:

$$T_0 = \frac{4r_0}{(1+r_0)^2}, \tag{7}$$

$$R_0 = 1 - T_0 = \left[\frac{1-r_0}{1+r_0}\right]^2, \tag{8}$$

$$\alpha = \frac{4\Gamma_L\Gamma_R}{\Gamma^2}, \tag{9}$$

$$\bar{\Gamma} = \frac{\Gamma}{1+r_0}, \tag{10}$$

where $r_0=\pi^2 N_0^2 |t_0|^2$. Here, T_0 is the transmission function when the QD is disconnected from the left and right reservoirs, i.e., $t_L=t_R=0$. The current through the QD and AB arm is found below.

$$i_{\text{QD}} = \left[-\alpha\bar{\Gamma}\sqrt{R_0} - 2T_0\Gamma_L\Gamma_R \sin^2(\varphi_{AB}) - \frac{\Gamma_L-\Gamma_R}{2}\sqrt{\alpha T_0}\sin(\varphi_{AB})\right]\text{Im}[G^R_{dd}]\Delta f - \bar{\Gamma}\sqrt{\alpha T_0}\cos(\varphi_{AB})\text{Re}[G^R_{dd}]\Delta f - i_{\text{Ring}}, \tag{11}$$

$$i_{\text{AB}} = \left[\alpha\bar{\Gamma}\sqrt{T_0}(\sqrt{T_0}\cos^2(\varphi_{AB}) - 1) + 2T_0\Gamma_L\Gamma_R\sin^2(\varphi_{AB}) + \frac{\Gamma_L-\Gamma_R}{2}\sqrt{\alpha T_0}\sin(\varphi_{AB})\right]\text{Im}[G^R_{dd}]\Delta f + 2T_0\bar{\Gamma}\sqrt{\alpha}\cos(\varphi_{AB})\text{Re}[G^R_{dd}]\Delta f + i_{\text{Ring}} + T_0\Delta f. \tag{12}$$

In our analysis, we find that there exists a ring current even at zero bias,

$$i_{\text{Ring}} = -\sqrt{\alpha T_0}\Gamma \sin\varphi_{AB}\,\text{Im}[G^R_{dd}]\bar{f}. \tag{13}$$

Here, $\bar{f}=(f_L+f_R)/2$ is the average Fermi function. This current flows in the clockwise direction through the AB ring, and persists even at zero bias since it is proportional to $\bar{f}$, not Δf. Although the ring current can be of the same order of magnitude as the total current, it does not contribute to the source-drain current.

Using Eq. (6), we arrive at the exact transmission function,

$$T(\epsilon) = T_0 - 2\bar{\Gamma}\sqrt{\alpha T_0 R_0}\cos(\varphi_{AB})\text{Re}[G^R_{dd}(\epsilon)] - \bar{\Gamma}\{\alpha[1 - T_0\cos^2(\varphi_{AB})] - T_0\}\text{Im}[G^R_{dd}(\epsilon)]. \tag{14}$$

We emphasize that $G^R_{dd}(\epsilon)$ is the full interacting QD retarded Green function, and Eq. (14) applies to systems with an interacting QD.

B. Noninteracting limit

In the noninteracting limit, we will address two important points. First, as the coupling to the left and right reservoirs is increased through $|t_0|$, the electron becomes more localized

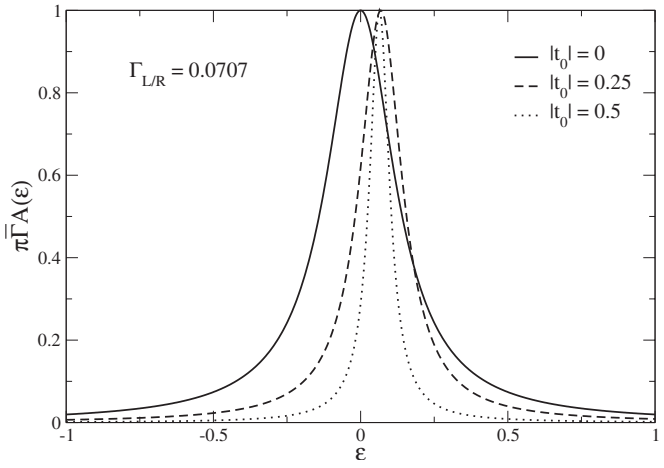

FIG. 2. QD spectral function for different magnitudes of $|t_0|$ at $\varphi_{AB}=0$. As $|t_0|$ is increased, the electron becomes more localized on the QD and the distribution of energies shifts away from the Fermi energy.

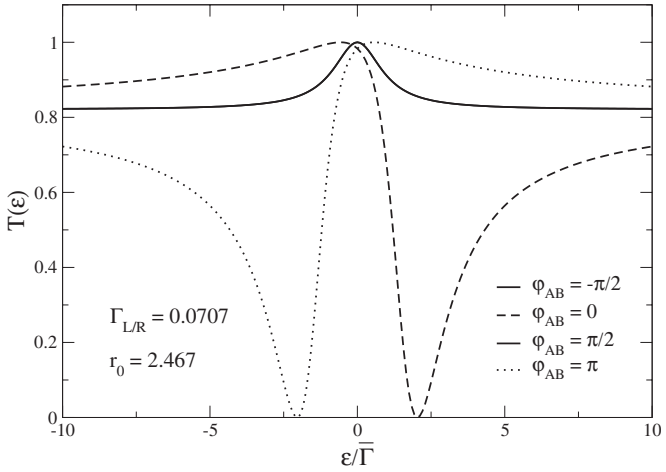

FIG. 3. Noninteracting transmission function for different values of φ_{AB}. When $\varphi_{AB}=(-\frac{\pi}{2},\frac{\pi}{2})$, we see a resonance at the QD energy level. The $\varphi_{AB}=(-\frac{\pi}{2},\frac{\pi}{2})$ curves coincide; away from these curves, the interference effects become more pronounced and the transmission function becomes asymmetrical. When $\varphi_{AB}=(0,\pi)$, the interference effects become most pronounced and a very strong antiresonance emerges, which is shifted to the left or right of the QD energy level. In the limit $|\epsilon|\to\infty$, the transmission converges to a finite value, due to the AB arm.

on the QD. Second, the noninteracting system is not suitable for controlling both charge and spin transport.

The noninteracting QD spectral function is given by

$$A(\epsilon) = \frac{\bar{\Gamma}/\pi}{(\epsilon - \epsilon_d - \delta)^2 + \bar{\Gamma}^2}, \tag{15}$$

where

$$\delta = \frac{2\sqrt{r_0\Gamma_L\Gamma_R}}{1+r_0}\cos(\varphi_{AB}) \tag{16}$$

and $\bar{\Gamma}$ was defined in Eq. (10). We plot $A(\epsilon)$ in Fig. 2 for different values of $|t_0|$. Notice that as the magnitude of $|t_0|$ is increased, the QD spectral function becomes sharper and the center of the peak is shifted. This shift in the QD energy, δ, and the reduced line broadening, $\bar{\Gamma}$, are easily understood by performing a bonding-antibonding transformation of the leads in real space. Upon doing so, the QD is now only coupled to the first site of the bonding chain, where the local energy of this site is shifted by $-|t_0|\cos(\varphi_{AB})$. Thus, by increasing $|t_0|$, the connection of the QD to the bonding chain is reduced, and the energy level of the QD is shifted upward.

The differential conductance is given as $G(\Phi)=e(dI/d\Phi)$, and in the zero bias and low-temperature limit, $G(0)=\frac{2e^2}{h}T(0)$. Therefore, at equilibrium, we only need $T(0)$ to determine the conductance. In Fig. 3, we plot the transmission amplitude as a function of the AB phase, φ_{AB}. When $\varphi_{AB}=\pm\frac{\pi}{2}$, $T(0)=1$. When $\varphi_{AB}=(0,\pi)$, the Fano antiresonance becomes most prominent and the minimum of the peaks are positioned significantly above and below the Fermi energy. As a result of this fact, we are not able to extinguish the charge or spin conductance at zero bias. If we were able to shift the minima of these antiresonance peaks to the Fermi energy, then we would be able to fully control the transport through this system at zero bias by tuning φ_{AB}. In the next section, we show that we can accomplish this through the Kondo effect.

C. Interacting Fano effect

When a local many-body interaction is present on the QD site, the problem is essentially reduced to calculating the full QD retarded Green function, $G^R_{dd}(\epsilon)$. Once we know this Green function, we may then calculate the transmission function using Eq. (14). In this paper, we take into account the Coulomb interaction on the QD in the form of the Anderson interaction,

$$\mathcal{H}_{int} = U\hat{n}_{d\uparrow}\hat{n}_{d\downarrow}. \tag{17}$$

We perform the diagrammatic calculation in the imaginary-time formalism. The QD Green function, at imaginary Matsubara frequency $i\omega_n=i\frac{(2n+1)\pi}{\beta}$, is given by $G_{dd}(i\omega_n)=[G^0_{dd}(i\omega_n)^{-1}-\Sigma(i\omega_n)]^{-1}$, where the self-energy $\Sigma(i\omega_n)$ is calculated to second order in U (Fig. 4). The second-order perturbation theory has been studied extensively[17–21] and shown to be a very good approximation in the particle-hole symmetric limit up to values of $U/\bar{\Gamma}\simeq 6$ (weak-coupling regime). This weak-coupling approximation has also been used within the framework of dynamical mean field theory,[22] and produced agreement with nonperturbative methods. In our model, the particle-hole symmetry is broken for $\delta\neq 0$, but the calculation of the zero bias conductance is in excellent agreement with the nonperturbative numerical renormalization group[3] (NRG) as will be shown.

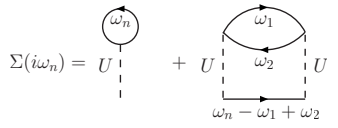

FIG. 4. Self-energy expanded to second order in U.

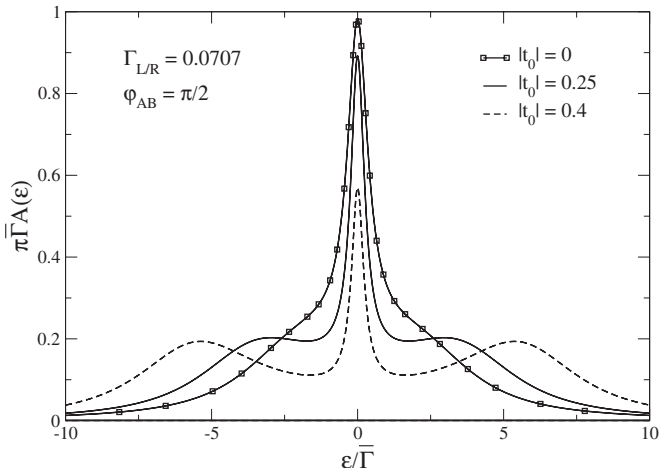

FIG. 5. Interacting QD spectral function for different magnitudes of $|t_0|$ when $\varphi_{AB}=\frac{\pi}{2}$, $U=0.6$, and $\beta=160$. We see that as $|t_0|$ is increased, the electron becomes more localized on the QD and, as a result, the correlations due to the Coulomb interaction become more pronounced.

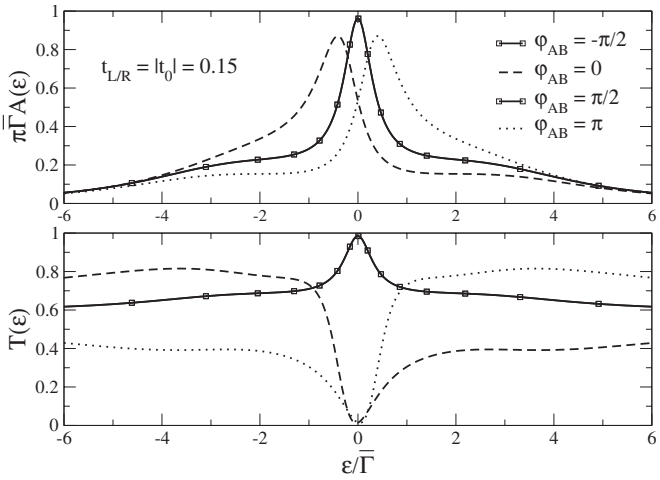

FIG. 6. QD spectral function and transmission amplitude for $U=0.6$ and $\beta=160$. The $\varphi_{AB}=\frac{\pi}{2}$ and $\frac{-\pi}{2}$ curves are identical, and at these values, the spectral function is symmetric and the transmission amplitude displays resonant behavior. On the other hand, when $\varphi_{AB}=0$ and π, the spectral function is asymmetric and the transmission amplitude has an antiresonance.

The first-order diagram becomes $U\langle n_d\rangle=\frac{U}{2}$ in the half-filled limit. Absorbing the first-order diagram into the noninteracting Matsubara Green function, we have

$$G_{dd}^0(i\omega_n) = \frac{1}{i\omega_n - \delta + i\bar{\Gamma}\,\mathrm{sign}(\omega_n)}, \tag{18}$$

and the second-order self-energy becomes

$$\Sigma^{(2)}(i\omega_n) = \frac{U^2}{\beta^2}\sum_{\omega_1,\omega_2} G_{dd}^0(i\omega_n - i\omega_1)G_{dd}^0(i\omega_2)G_{dd}^0(i\omega_1 + i\omega_2). \tag{19}$$

Now we are in position to solve this problem numerically. First, we calculate the self-energy in Matsubara frequency. Then in order to calculate $T(\epsilon)$, we must analytically continue the Green function to its retarded form in real frequency space, $G_{dd}(i\omega_n \to \epsilon + i\eta)$. For the numerical analytical continuation, we used the N-point Padé approximant method.[23]

Let us first look at the spectral function, $A(\epsilon)=-\frac{1}{\pi}\,\mathrm{Im}[G_{dd}(\epsilon)]$. For the resonant case ($\varphi_{AB}=\frac{\pi}{2}$), the spectral function is plotted for different values of $|t_0|$ in Fig. 5. We see that as we increase the coupling $|t_0|$ of the L, R states to the AB arm, the effective many-body interaction $U/\bar{\Gamma}$ is strongly enhanced. From our analysis of the noninteracting system, this is exactly what we expected to happen. When $|t_0|=0$, we start in the weakly interacting valence fluctuating regime, but as we increase $|t_0|$ to 0.4, the Kondo peak at zero frequency and the Hubbard satellites[24] emerge.

The transmission functions are given in Fig. 6. As in the noninteracting case, we have resonance (antiresonance) phenomena at $\varphi_{AB}=-\frac{\pi}{2},\frac{\pi}{2}$ $(0,\pi)$, respectively. The antiresonance peaks are known as the Fano-Kondo antiresonance, and have been observed experimentally in a quantum wire with a side coupled QD.[8,9] For $\varphi_{AB}=0$ and π, the antiresonance peaks are antisymmetric of one another about the Fermi energy.

Now let us examine the zero bias conductance. Our results are given in Fig. 7 as a function of φ_{AB} for different values of the ratio $|t_0|/t_{L/R}$. The NRG calculation of Ref. 3 examined the zero bias conductance as a function of φ_{AB} for different values of the gate potential, ϵ_d. A careful straightforward identification of the model parameters shows that our results agree excellently with the NRG,[25] which justifies our self-energy approximation. Since $G(0)$ is only dependent on the value of the Green function at the Fermi energy, this implies that the second-order self-energy approximation at least produces reliable results near the Fermi energy for $\delta \neq 0$.

From Fig. 7, we see that $G(0)$ oscillates as a function of φ_{AB} and that the magnitude of these oscillations is strongly

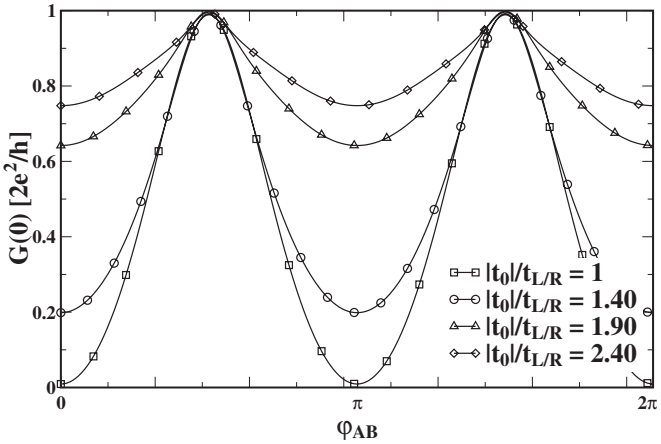

FIG. 7. Zero bias conductance as a function of φ_{AB} for $t_L=t_R=0.15$, $U=0.5$, and $\beta=160$. The conductance approaches unity when $\varphi_{AB}=\frac{2n+1}{2}\pi$. Conversely, the conductance approaches a minimum when $\varphi_{AB}=n\pi$, with integer n.

dependent on the ratio $|t_0|/t_{L/R}$. We find that $|t_0|/t_{L/R}=1$ is a special case which maximizes the magnitude of the AB oscillations. These oscillations are a consequence of the $\cos^2(\varphi_{AB})$ term in Eq. (14) and the sharp feature near the Fermi energy of the spectral function (Fig. 6). The resonance $[G(0)=\max]$ (antiresonance $[G(0)=\min]$) peaks occur at $\varphi_{AB}=\frac{2n+1}{2}\pi(n\pi)$, with integer n. Thus, by tuning φ_{AB}, we may filter the charge through the system at zero voltage bias. The reason why we have so much control over the conductance at zero bias is due to the Kondo effect. The Kondo effect induces a sharp peak near the Fermi energy in the spectral function, insensitive to φ_{AB}. This feature is due to the many-body effect and is not present in the noninteracting case (Fig. 3).

D. Spin transport

For a single orbital QD, the addition of the spin-orbit interaction induces a spin dependent phase in t_R,[2] i.e., $t_R \rightarrow t_R e^{-i\sigma\varphi_{SO}}$, where $\sigma=+$ $(-)$ for spin up (down). Unlike φ_{AB} which arises from the orbital motion, φ_{SO} depends on the spin. To simplify our Hamiltonian, we make the unitary transformation

$$c_{Rk}^{\dagger} \rightarrow e^{is\varphi_{SO}} c_{Rk}^{\dagger} \tag{20}$$

so that

$$t_0 \rightarrow e^{is\varphi_{SO}} t_0. \tag{21}$$

Now we define a spin dependent AB tunneling coefficient

$$t_{0\sigma} = |t_0| e^{i(\varphi_{AB}+\sigma\varphi_{SO})}. \tag{22}$$

As a result of the spin dependence in $t_{0\sigma}$, the Green's functions also gain a spin dependence and the spin dependent second-order self-energy is given by

$$\Sigma_{\sigma}^{(2)}(i\omega_n) = \frac{U^2}{\beta^2} \sum_{\omega_1,\omega_2} G_{dd\sigma}^{0}(i\omega_n - i\omega_1) \times G_{dd-\sigma}^{0}(i\omega_2) G_{dd-\sigma}^{0}(i\omega_1 + i\omega_2). \tag{23}$$

Now let us examine the spectral and transmission functions given in Fig. 8. As in the spin independent case, we see resonance and antiresonance behaviors in the transmission function. More importantly, due to the SO interaction, we now have two phase factors, φ_{AB} and φ_{SO}, which, along with the Kondo resonance near the Fermi energy, we may use to filter the spin up and spin down electrons independently.

Let us take a closer look at Fig. 8. We see that when $\varphi_{AB}=\varphi_{SO}=\frac{\pi}{4}$, $A_{\uparrow}$ has a spectral structure similar to that of a Kondo dot, while $A_{\downarrow}$ develops a slight asymmetry from the spin up case. Looking at the transmission function, $T_{\uparrow}$ is similar in shape to its spectral function and $T_{\uparrow}$ shows strong antiresonance behavior due to the AB ring. This mechanism gives us a strong control on the spin transport. At the Fermi energy, $T_{\uparrow}(0)\cong 1$ and $T_{\downarrow}\cong 0$. When $\varphi_{SO}=\frac{\pi}{8}$, both $T_{\uparrow}$ and $T_{\downarrow}$ show strong interference effects.

To look at the zero bias spin conductance, we turn to Fig. 9, where we show the SO oscillations of the zero bias conductance. The behavior of the spin up and spin down conductances is a result of the $\cos^2(\varphi_{AB}+\varphi_{SO})$ term for spin up and the $\cos^2(\varphi_{AB}-\varphi_{SO})$ term for spin down in Eq. (14). In the figure, we see that when $\varphi_{AB}=\frac{\pi}{4}$, the spin-polarized conductance $(\eta=[G_{\uparrow}(0)-G_{\downarrow}(0)]/[G_{\uparrow}(0)+G_{\downarrow}(0)])$ is maximized. Conversely, when $\varphi_{SO}=\frac{\pi}{2}$, the spin polarization is suppressed.

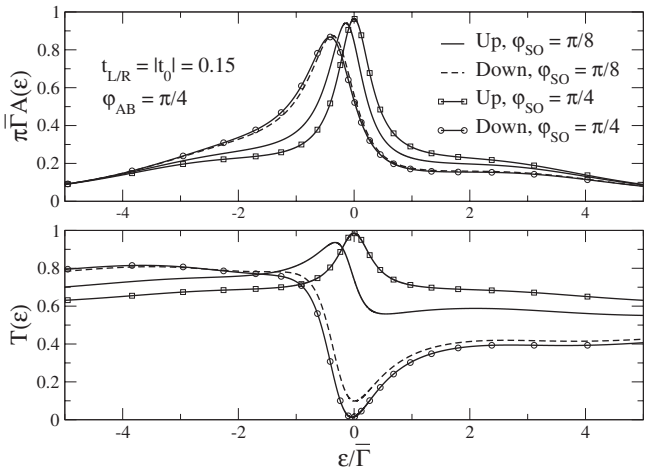

FIG. 8. Spin dependent spectral and transmission functions for $\varphi_{SO}=\frac{\pi}{8}$ and $\frac{\pi}{4}$, $U=0.6$, and $\beta=160$. For $\varphi_{SO}=\frac{\pi}{4}$, $A_{\uparrow}$ $(A_{\downarrow})$ is symmetric (asymmetric), while $T_{\uparrow}$ $(T_{\downarrow})$ displays resonance (antiresonance) behavior. In addition, $T_{\uparrow}(0)\sim 1$ and $T_{\downarrow}(0)\sim 0$. For $\varphi_{SO}=\frac{\pi}{8}$, both $A_{\uparrow}$ and $A_{\downarrow}$ are asymmetrical and $A_{\downarrow}$ lies on the curve of $A_{\downarrow}(\varphi_{SO}=\frac{\pi}{4})$. $T_{\uparrow}$ and $T_{\downarrow}$ both display antiresonant phenomena.

The most important results of this paper are shown in the spin-polarized conductance in Fig. 10. Here, we plot η as a function of φ_{SO} for different values of φ_{AB}. The maximum in the spin up or spin down conductance occurs approximately when $\varphi_{AB}\pm\varphi_{SO}=\frac{2n+1}{2}\pi$, while the minimum occurs at $\varphi_{AB}\pm\varphi_{SO}=m\pi$. This can be seen from the $\cos^2(\varphi)$ factor in Eq. (14), since at the Kondo resonance $(\epsilon\approx 0)$ only T_0 and the term proportional to $\mathrm{Im}[G_{dd}^{R}(\epsilon)]$ become relevant. Therefore, the necessary conditions on φ_{SO} and φ_{AB} for maximum or minimum spin-polarized conductance are

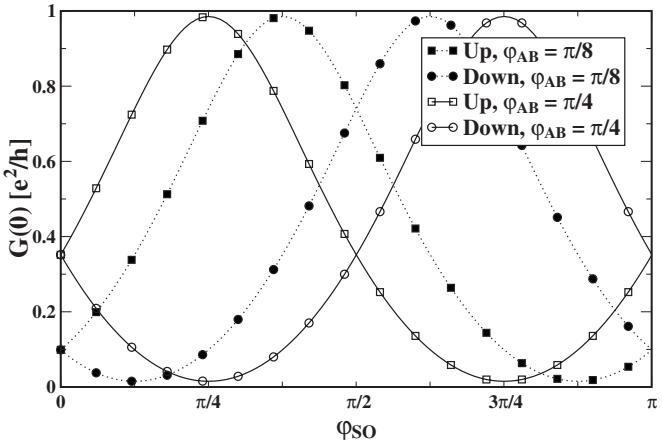

FIG. 9. SO oscillations for $\varphi_{AB}=\frac{\pi}{8}$ and $\frac{\pi}{4}$, $U=0.6$, and $\beta=160$. The minima and maxima of the SO oscillations approach 0 and 1, respectively.

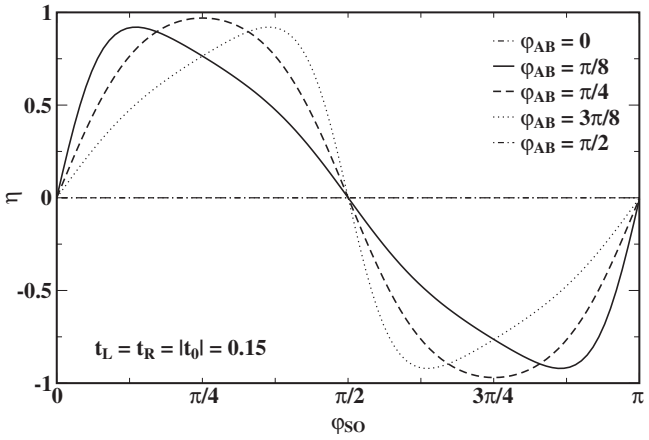

FIG. 10. Spin-polarized conductance for different AB phases when $U=0.6$ and $\beta=160$. Here, the spin polarization is defined as $\eta=[G_{\uparrow}(0)-G_{\downarrow}(0)]/[G_{\uparrow}(0)+G_{\downarrow}(0)]$. We see that the spin polarization may be fully controlled by tuning φ_{AB} and φ_{SO}. The $\varphi_{AB}=0$ and $\frac{\pi}{2}$ curves are identical.

$$\left(\frac{\varphi_{SO}}{\varphi_{AB}}\right)_{\eta\approx 1} = \frac{n-m+\frac{1}{2}}{n+m+\frac{1}{2}}, \tag{24}$$

$$\left(\frac{\varphi_{SO}}{\varphi_{AB}}\right)_{\eta\approx 0} = \frac{n-m}{n+m+1}. \tag{25}$$

Here, again we emphasize the crucial role which the many-body interactions play in this system. The Kondo effect serves to simultaneously pin the resonance or antiresonance peaks of the spin dependent conductance at the chemical potential, as seen in Fig. 6. As a result, when the SO interaction is turned on, we gain complete control over the spin polarization (Fig. 10). Furthermore, even if there only exists a small SO interaction in the QD, this device serves to enhance those inherent SO effects. In contrast to this, in the noninteracting device (Fig. 3) the resonance or antiresonance peaks occur at significantly different energies, making it impractical to use as a spin or charge filter. Therefore, we have shown that the QD-ABI is an ideal spin filter where neither a voltage bias nor a gate potential is needed.

III. CONCLUSION

In this paper, we have shown that the QD-ABI may be used to localize and delocalize electrons on the QD. As a result, when the QD is strongly correlated, we can effectively control the strength of these correlations through the magnitude of t_0. With larger t_0, electrons get more localized on the QD. In the case of a Coulomb interaction on the QD, the Kondo effect induces a sharp peak in the spectral function near the Fermi energy. We emphasize that the exact relation for the transmission [Eq. (14)] shows that the resonance or antiresonance is driven by the AB phase factor once the spectral function develops a sharp feature near the Fermi energy, independent of its many-body character.

The most important result of this paper is realized when a SO interaction is present on the QD in addition to the Coulomb interaction. In this case, the Kondo peak and the spin dependent $\cos^2(\varphi)$ term induce the resonance or antiresonance in the zero bias spin dependent conductance. Due to this property, we can vary the $G_{\uparrow}(0)$ and $G_{\downarrow}(0)$ between 0 and e^2/h. Further, the SO phase gives us another degree of freedom, in addition to the AB phase, so that the spin up and spin down conductances may be varied independently. Thus, by tuning φ_{AB} and φ_{SO}, the spin polarization may be fully controlled in the QD-ABI.

APPENDIX: DERIVATION OF $T(\epsilon)$

In this appendix, we present the full derivation of the transmission function. The transmission is given in terms of Keldysh Green functions,

$$T(\epsilon)\Delta f = i_{\mathrm{QD}}(\epsilon) + i_{\mathrm{AB}}(\epsilon), \tag{A1}$$

$$i_{\mathrm{QD}}(\epsilon) = -t_L[G^<_{dL}(\epsilon) - G^<_{Ld}(\epsilon)], \tag{A2}$$

$$i_{\mathrm{AB}}(\epsilon) = [-t_0^* G^<_{RL}(\epsilon) + t_0 G^<_{LR}(\epsilon)], \tag{A3}$$

where $G^<_{dL}$ and $G^<_{RL}$ are the Fourier transforms of the following time dependent nonequilibrium Green functions (NEGFs):

$$G^<_{dL}(t) = \frac{1}{\sqrt{\Omega}}\sum_k i\langle d^\dagger(0)c_{Lk}(t)\rangle, \tag{A4}$$

$$G^<_{RL}(t) = \frac{1}{\Omega}\sum_{kk'} i\langle c^\dagger_{Lk}(0)c_{Lk'}(t)\rangle, \tag{A5}$$

and $G^<_{Ld}=-(G^<_{dL})^*$ and $G^<_{LR}=-(G^<_{RL})^*$. In calculating these Green functions, it becomes convenient to disconnect the QD from the reservoirs, i.e., $t_L=t_R=0$, and define the following QD-excluded Green functions:

$$g^r_{LL} = g^r_{RR} = \frac{-i\pi N_0}{1+r_0}, \tag{A6}$$

$$g^r_{RL} = (g^r_{LR})^* = \frac{\pi^2 N_0^2 t_0}{1+r_0}, \tag{A7}$$

$$g^<_{LL} = \frac{2\pi i N_0}{(1+r_0)^2}(f_L + r_0 f_R), \tag{A8}$$

$$g^<_{RR} = \frac{2\pi i N_0}{(1+r_0)^2}(f_R + r_0 f_L), \tag{A9}$$

$$g^<_{RL} = -(g^<_{LR})^* = \frac{-2\pi^2 N_0^2}{(1+r_0)^2} t_0 (f_L - f_R). \tag{A10}$$

We express $G^<_{dL}$ and $G^<_{RL}$ in terms of the fully interacting retarded and advance QD Green functions and the above QD-excluded noninteracting NEGFs.

To simplify our notation, we define $F^r_{\alpha d}$, $F^a_{\alpha d}$, and $F^<_{\alpha d}$, which are the retarded, advanced, and lesser Green functions

which describe the transport from the QD to the α lead in terms of the QD-excluded Green functions.

$$F^r_{Ld} = (F^a_{dL})^* = t_L(t_L g_{LL} + t_R g_{LR})^r = \frac{1}{1+r_0}(-i\Gamma_L + \sqrt{r_0\Gamma_L\Gamma_R}e^{-i\varphi_{AB}}), \tag{A11}$$

$$F^r_{Rd} = (F^a_{dR})^* = t_R(t_R g_{RR} + t_L g_{RL})^r = \frac{1}{1+r_0}(-i\Gamma_R + \sqrt{r_0\Gamma_L\Gamma_R}e^{i\varphi_{AB}}), \tag{A12}$$

$$F^<_{Ld} = -(F^<_{dL})^* = t_L(t_L g_{LL} + t_R g_{LR})^< = \frac{2}{1+r_0}[i\Gamma_L(f_L + r_0 f_R) + \sqrt{r_0\Gamma_L\Gamma_R}e^{-i\varphi_{AB}}(f_L - f_R)], \tag{A13}$$

$$F^<_{Rd} = -(F^<_{dR})^* = t_R(t_R g_{RR} + t_L g_{RL})^< = \frac{2}{1+r_0}[i\Gamma_R(f_R + r_0 f_L) + \sqrt{r_0\Gamma_L\Gamma_R}e^{i\varphi_{AB}}(f_R - f_L)]. \tag{A14}$$

Therefore, G_{RL} and G_{dL} may be written in terms of F's and the full QD Green function as

$$t_L t_R G_{RL} = F_{Rd} G_{dd} F_{dL}, \tag{A15}$$

$$-t_L G_{dL} = G_{dd} F_{dL}. \tag{A16}$$

Using the Keldysh Green function relations[26]

$$(AB)^< = A^< B^a + A^r B^<, \tag{A17}$$

$$(ABC)^< = A^< B^a C^a + A^r B^< C^a + A^r B^r C^<, \tag{A18}$$

the lesser Green functions become

$$G^<_{RL} = F^<_{Rd} G^a_{dd} F^a_{Ld} + F^r_{Rd} G^<_{dd} F^a_{Ld} + F^<_{Rd} G^a_{dd} F^a_{Ld}, \tag{A19}$$

$$-t_L G^<_{dL} = G^<_{dd} F^a_{dL} + G^r_{dd} F^<_{dL}. \tag{A20}$$

Making use of the nonequilibrium steady state condition, $i_L + i_R = 0$, we may construct $G^<_{dd}$ in terms of G^r_{dd} and G^a_{dd} as follows. The ensemble averaged currents are given by

$$i_\alpha = -t_\alpha(G^<_{d\alpha} - G^<_{\alpha d}) = (F^a_{d\alpha} - F^r_{\alpha d})G^<_{dd} + G^r_{dd}F^<_{d\alpha} + F^<_{\alpha d}G^a_{dd}, \tag{A21}$$

where $\alpha = (L,R)$. Therefore, by invoking the steady state condition, the QD lesser Green function becomes

$$G^<_{dd} = \frac{(F^<_{dL} + F^<_{dR})G^r_{dd} - (F^<_{Ld} + F^<_{Rd})G^a_{dd}}{(F^r_{Ld} - F^a_{dL}) + (F^r_{Rd} - F^a_{dR})}. \tag{A22}$$

Inserting $G^<_{dd}$ into Eq. (A21) with $\alpha = L$, we arrive at i_{QD} [Eq. (11)]. The current through the AB arm is given by

$$\begin{aligned} t_L t_R i_{AB} = t_L t_R(-t_0^* G^<_{RL} + t_0 G^<_{LR}) &= (-t_0^* F^r_{Rd} F^<_{dL} + t_0 F^r_{Ld} F^<_{dR})G^r_{dd} \\ &+ (-t_0^* F^<_{Rd} F^a_{dL} + t_0 F^<_{Ld} F^a_{dR})G^a_{dd} \\ &+ (-t_0^* F^r_{Rd} F^a_{dL} + t_0 F^r_{Ld} F^a_{dR})G^<_{dd}, \end{aligned} \tag{A23}$$

where all of the terms have been solved for. Thus, after doing some algebra, i_{AB} may be expressed as Eq. (12). Using Eq. (6), we arrive at the transmission function [Eq. (14)].

[1] Qing-feng Sun and X. C. Xie, Phys. Rev. B **73**, 235301 (2006).
[2] Qing-feng Sun, Jian Wang, and Hong Guo, Phys. Rev. B **71**, 165310 (2005).
[3] W. Hofstetter, J. Konig, and H. Schoeller, Phys. Rev. Lett. **87**, 156803 (2001).
[4] Tae-Suk Kim and S. Hershfield, Phys. Rev. Lett. **88**, 136601 (2002).
[5] Rosa López, David Sánchez, and Llorenç Serra, Phys. Rev. B **76**, 035307 (2007).
[6] U. Fano, Phys. Rev. **124**, 1866 (1961).
[7] J. Gores, D. Goldhaber-Gordon, S. Heemeyer, M. A. Kastner, H. Shtrikman, D. Mahalu, and U. Meirav, Phys. Rev. B **62**, 2188 (2000).
[8] Kensuke Kobayashi, Hisashi Aikawa, Akira Sano, Shingo Katsumoto, and Yasuhiro Iye, Phys. Rev. B **70**, 035319 (2004).
[9] Masahiro Sato, Hisashi Aikawa, Kensuke Kobayashi, Shingo Katsumoto, and Yasuhiro Iye, Phys. Rev. Lett. **95**, 066801 (2005).
[10] J. Kim, J. R. Kim, Jeong-O Lee, J. W. Park, H. M. So, N. Kim, K. Kang, K. H. Yoo, and J. J. Kim, Phys. Rev. Lett. **90**, 166403 (2003).
[11] E. I. Rashba, Fiz. Tverd. Tela (Leningrad) **2**, 1224 (1960) [Sov. Phys. Solid State **2**, 1109 (1960)].
[12] M. Dobers, J. P. Vieren, Y. Guldner, P. Bove, F. Omnes, and M. Razeghi, Phys. Rev. B **40**, 8075 (1989); T. Kita, Y. Sato, S. Gozu, and S. Yamada, Physica B **298**, 65 (2001); Y. S. Gui, C. M. Hu, Z. H. Chen, G. Z. Zheng, S. L. Guo, J. H. Chu, J. X. Chen, and A. Z. Li, Phys. Rev. B **61**, 7237 (2000).
[13] Kensuke Kobayashi, Hisashi Aikawa, Shingo Katsumoto, and Yasuhiro Iye, Phys. Rev. Lett. **88**, 256806 (2002).
[14] Yigal Meir and Ned S. Wingreen, Phys. Rev. Lett. **68**, 2512 (1992).
[15] S. Datta, *Electronic Transport in Mesoscopic Systems* (Cambridge University Press, Cambridge, England, 1995).
[16] J. Rammer and H. Smith, Rev. Mod. Phys. **58**, 323 (1986).
[17] K. Yosida and K. Yamada, Prog. Theor. Phys. **46**, 244 (1970).
[18] K. Yosida and K. Yamada, Prog. Theor. Phys. **53**, 1286 (1975).
[19] K. Yamada, Prog. Theor. Phys. **53**, 970 (1975).
[20] M. Salomaa, Solid State Commun. **38**, 815 (1981).
[21] V. Zlatić, B. Horvatić, and D. Sokcević, Z. Phys. B: Condens. Matter **59**, 151 (1985).
[22] Antoine Georges, Gabriel Kotliar, Werner Krauth, and Marcelo J. Rozenberg, Rev. Mod. Phys. **68**, 13 (1996).
[23] H. J. Vidberg and J. W. Serene, J. Low Temp. Phys. **29**, 179

(1977).
[24] B. Horvatić, D. Šokčević, and V. Zlatić, Phys. Rev. B **36**, 675 (1987).
[25] The percent difference between $G(0)$ $[|t_0|/t_{L/R}=1.90]$ calculated using second-order perturbation theory and the exact numerical renormalization group is $<4\%$ for all φ_{AB}. Here, the asymmetry is as large as $\delta/\bar{\Gamma}=0.895$.
[26] David C. Langreth and John W. Wilkins, Phys. Rev. B **6**, 3189 (1972).